ISSN: 2287-6898
International
Journal of Bio-Pharma Research
Volume 8, Issue 5 (2019) pp. 2575-2581
Research Article
Open Access

Ferroelctric behaviour of Fe_2O_3Zn Nnaocomposites

Kavin Micheal M.[1], Ayeshamariam A.[1,2*], Alhaji N.M.I.[3], Fowziya S.A.[3], Rajasekar S.[4] and M. Jayachandran[5]

[1]Department of Physics, Khadir Mohideen College, Adirampattinam, 614701, India.
[2]Research and Development Center, Bharathidasan University, Tiruchirappalli, 620 024, India.
[3]Department of Chemistry, Khadir Mohideen College, Adirampattinam, 614701, India.
[4]Department of Physics, Syed Ammal Engineering College, Ramanathapuram, 623501, India.
[5]Department of Physics, Sethu Institute of Technology, Pulloor, Kariyapatti, 626 106, India.

Abstract: The Zn doped Fe_2O_3 thin films are sprayed on the glass plate by the method of Spray analysis. Thin film was characterized by X-Ray diffractometer to study the crystal structure of the thin film. The average size of the calculated crystal size by using Scherer equation is 59 nm. Mixed metal oxides having spinel structure shows interesting structural properties. The completions of formation of spinel phase were identified using X-ray diffraction technique. All the compounds exhibit Rhombohedral spinel symmetry and lattice constant shows an irregular trend with substitution of Zn. Infra-red spectral studies shows an two strong bands, one around 600 cm^{-1} which is attributed to the intrinsic vibrations of Rhombohedral complexes and the other at 400 cm^{-1} is due to octahedral one. The morphology and size of the particles was found out by scanning electron microscopy while the elemental compositions by elemental EDAX analysis. The various compounds of the present system Fe_2O_3Zn were also investigated for their electronic studies.

Key words: Fe_2O_3Zn, X-ray diffractometer, Scanning Electron Microscopy and Hysteresis curve

Introduction

In past years, to eradicate organic pollutants from water which is waste conservative physical treatment and biological methods have been the main-stream techniques with varying degrees of success. So far, conventional methods such as adsorption on activated carbon, coagulation, microbial degradation, incineration, sedimentation and filtration have been used to treat wastewater [1]. Each process has some shortcomings. Different physical methods such as the membrane filtration processes (reverse osmosis, nanofiltration and electrodialysis etc.) are widely used. The major difficulty of the membrane method is that they have a limited lifetime before membrane fouling occurs and the periodic replacement of the membrane makes this method economically not viable. The most frequently and generally used disinfection method is Chlorination. However, chlorination-based water disinfection process may form potentially toxic disinfection by products, such as trihalomethanes and these are carcinogenic and mutagenic to the health of human [2-4].

Ozonaton is considered as a better water treatment process over chlorination since it avoids the formation of disinfection byproducts associated with chlorinated organic compounds. However, recently it has been discovered that ozone can generate cancer causing agent [5]. Conventional chemical oxidation processes [6-9] involve wet chemical oxidizing agents, including persulfate and Fenton reagents (Fe^{2+}/H_2O_2). These methods have been proven effective in the remediation of a wide array of organics, but have several disadvantages. These include potential safety hazards and toxicity of the strongly oxidizing agents (like H_2O_2 or permanganate). Also their high reactivity can lead to a short lifetime and thus incomplete oxidation of organics, producing intermediates that may be more toxic than the original pollutant [10]. These conventional methods prove to be uneconomic and insufficient for handling of effluents because, either they fail to achieve complete removal of pollutant [11] or of high operating costs. Moreover, they have further

Corresponding Author:
Dr. A. Ayeshamariam,
Head, Department of Physics
Khadir Mohideen College,
Adirampattinam-614701, Tamilnadu, India.
E-mail: aamariam786@gmail.com

drawbacks since they simply transfer the pollutants to another phase and produce large volume of sludge which itself requires treatment [12].

The development of chemical solution deposition processes for iron oxide thin films dates to the mid 1980s. H. Yang et al, on the sol – gel processing of thin films of Fe_2O_3, a widely used Ferro electric material, were some of the first examples that demonstrated it was possible to obtain the desirable properties of Fe_2O_3 materials in thin film form. The early work by these investigators and others led to rapid expansion of the research. At about this same time, a number of small companies interested in the development of nonvolatile memories based on Fe_2O_3nthin films were started. For some of the companies did not commercialize any thin film products at the time, the work they carried out encouraged the participation of the researchers in the filed. This led to the evolution of these materials to the point that today they are appearing in a number of devices and continue o be developed for other applications [13].

Depending on the crystal structure, the centers of the positive and negative charges may not coincide without the applications of external field. Such crystals are said to possess a spontaneous polarization. When spontaneous polarization of the dielectric can be reversed by an Electric field it is called ferroelectrics [14]. Crystals can be classified into 32-point groups according to their crystallographic symmetry, and these groups can be divided into two classes, one with center of symmetry and the other without center of symmetry. There are 21 groups, which do not have a center of symmetry. In crystals belonging to 20 of these point groups, negative and positive charges are generated on the crystal surfaces when appropriate stresses are applied. These materials are known as piezoelectric. Pyroelectricity is the phenomenon whereby, due to temperature dependence of the spontaneous polarization, as the temperature of the crystal is changed; electric charges corresponding to the change of the spontaneous polarization appear on the surface of the crystal. Among the pyroelectric crystals whose spontaneous polarization can be reversed by an electric field (not exceeding the break down limit of the crystal) are called ferroelectrics [15].

The definitions of a ferroelectric are a material that exhibits one or more ferroelectric phases in a realizable range of temperature and pressure. In the ferroelectric phase, the crystal is spontaneously electrically polarized and the polarization has more than one possible equilibrium orientation. To establish ferroelectricity, it must be demonstrated that the polarize can be reoriented between orientation states by a realizable electric field. Ferroelectric materials are a sub-group of the pyroelectric class of materials, which in turn a sub-group of the piezoelectric class of materials. Ferroeelctrics, therefore, possess both piezoelectric and pyroelectric properties, in addition of their unique ferroelectric properties, in addition of their unique ferroelectric properties. In these ferroelectric materials, the direction of the spontaneous dipoles is parallel to each other in a crystal (polar crystals). There are cases in which antiparallel orientation lowers the dipole-dipole interaction energy. Such crystals are anti-polar crystals [16].

In an anti-polar crystal, where the free energy of an anti-polar state does not differ appreciably from that of a polar state, the application of an external electric field or mechanical stress may cuase a transition of the dipole orientation to the parallel state. Such crystals are called antiferroelectrics. In some cases, the free energies are so similar that it is possible to switch the antiferrolectric to a polar state by an external field or by a mechanical stress may cause a transition of the dipole orientation to a parallel state. Such crystals are called antiferroelctrics. In some cases, the free energies are so similar that it is possible to switch the antiferroelectric to a polar state by an external field or by a mechanical stress. Thus an antiferroelectric is characterized by the rows of dipoles, with the dipole moment of adjacent rows equal but anti parallel. This arrangement can be regarded as two inter penetrating sub lattices of equal and opposite polarization with no net spontaneous polarization [17].

The relationship between E (applied field) and P (induced polarization) in paraelectric, ferroelectric and antiferroelctric phases along with stress vs applied field in different material compositions. In paraelectric phase the P-E relation is linear; in a ferroelectric phase there appears a hysteresis caused by the transaction of the spontaneous polarization between the positive and negative directions; in an antiferroelctric phase, at low electric field, the induced polarization is proportional to E, and when E exceeds a certain

value E_{crit}, the crystal becomes ferroelectric (electric field induced phase transition), an d the polarization shows hysteresis with respect to E. After removal of the electric field, the crystal returns to its anti-polar state, and hence, no spontaneous polarization can be observed as whole. This is called double hysteresis curve.

Ferroelectric thin film devices have been studied for well over the thirty years since Wu *et al.,* demonstrated thin films could be integrated with other semiconductor devices. The continuing interest in this type of research is a consequence of the potentially numerous. Applications with these thin film compositions in microelectronic devices. Such as memories microelecro mechanical systems and electro optical applications. Antiferroelectric compositions also have potential applications in the areas of microelectronic and micro electro mechanical systems. In some of these cases antiferroelctric compositions offer an alternative to ferroelectric capacitors and transducers. U.I. Gaya *et al.,* [17] coined the term "soft" to describe those antiferroelctrics in which an attainable applied field can switch the direction polarization of sub lattice in opposes. Thin films of these materials are interesting because the breakdown strength of thin film typically surpasses by an order of magnitude bulk ceramics of the same composition. As a result devices based on phase switching may well be more robust and reliable in thin film form than in the bulk [18].

Since the capillary force causes the aforementioned stress concentration and the variation of pore sizes, the stress concentration should be reduced by the limiting the interaction between the liquid and the pore walls, and by methods that reduce the variation of pore sizes. Several methods have been proposed for this purpose including the use of surfactants, drying controlled chemical additives (DCCA), and hypercritical drying. A surfactant acts to reduce the capillary force so that it will reduce the stress concentration. In hypercritical drying, the film is dried by heating the gel under pressure to a point above the critical temperature and pressure to a point above the critical temperature and pressure of the solvent. In this process there is no capillary force. The hypercritical dried Gel has the same volume as the Sol from which it is made. Several kinds of chemicals have been used as DCCA including formamide and oxalic acid. Both formamide and oxalic acid produce larger and more uniform pores, which help to increase the permeability of the Gel. On the other hand, if the condensation reaction is retarded in the films, the evolved stress can be relieved by structural relaxation, allowing crack-free films to be formed [19].

Materials and Methods

The working solution of 0.1 M $FeCl_3.6H_2O$ was obtained by dissolving 0.15 gm of Zn $(CH_3COO)_2.2H_2O$ diluted in 50 ml of methanol and deionized water in 50 ml of deionized water. The starting solution was prayed on the glass plate which was placed on a substrate temperature of temperature 100° C. The distance between the nozzle and substrate was set to 10 cm. During the spraying process, the substrate was heated by electrically heating the glass plate. The dried powder was collected and then characterized by X-Ray diffractometer. The spinel phase formation of the oxides was confirmed by X-ray diffraction (PW1710 Philips diffractometer) with CuKα radiation (k = 1.54056 A°). The morphologies of the samples were characterized with a field emission scanning electron microscope (FE-SEM, JSM-6701F, JEOL Inc., Japan). Transmission electron microscopy (TEM, JEM-1230) operating at 200 kV was applied to characterize the morphology of Fe_2O_3Zn.

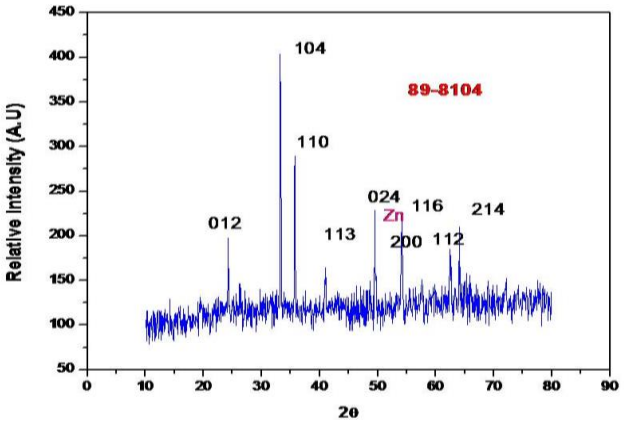

Figure 1: XRD analysis of Fe_2O_3/Zn

Results and Discussion

The X-Ray diffractometer is well matched with JCPDS file number of 89-8104, MW= 159.69, and its cell parameters a = 5.023 C = 13.708, the system is Rhombohedral, the calculated values of lattice parameters were well matched with JCPDS values, the values are a = 5.112 and c = 13.234. The structural calculations of observed and standard values were well matched one another is shown in Table 1 and Table 2. Its lattice parameter, crystal size and porosity were listed in Table 3.

Table 1: Structural studies of Fe_2O_3/Zn

d_{hkl}	d_{exp}	Strain $\frac{\Delta d}{d_o} = \left(\frac{d_{exp} - d_{hkl}}{d_{hkl}}\right)$	Rel.Int	Hkl
3.66883	3.6727	0.00105	28.04	012
2.69312	2.6919	-4.53006E-4	100.00	104
2.51229	2.5115	-3.14454E-4	58.46	110
2.20183	2.2009	-4.22376E-4	11.53	113
1.83886	1.8363	-0.00139	35.78	024
1.69322	16900	9979.98298	28.69	116
1.60000	1.5988	-7.5E-4	7.71	122
1.48508	1.4823	-0.00187	24.69	214
1.45222	1.4500	-0.00153	34.63	300

Table 2: Structural parameters and crystal size values of Fe_2O_3/Zn

Position	FWHM	Beta	Crystal size (nm)	Dislocation density (lines/m²)	Hkl
24.24(1)	1.83441	0.00183	79.103	1.59814E-4	012
33.240(4)	1.34656	0.00194	74..09	1.822E-4	104
35.710(6)	1.25615	0.0023	62.905	2.52714E-4	110
40.96(2)	1.10092	0.00399	36.258	7.60663E-4	113
49.530(8)	0.91943	0.00195	74.130	1.81975E-4	024
54.12(1)	0.84661	0.00392	36.899	7.34464E-4	116
57.56(4)	0.8	0.00558	25.945	0.00149	122
62.49(1)	0.74254	0.00249	58.057	2.96682E-4	214
64.069(7)	0.72611	0.00178	81.394	1.50944E-4	300

Table 3: Structural parameters and crystal size values of Fe_2O_3/Zn

Composition Fe_2O_3:Zn	Molecular Weight (gm)	Lattice parameter (A°)		Ave. Crystal Size (nm)	X-Ray density dx gm/cm³	Bulk Density dB gm/cm³	Porosity P (%) $1-\left[\frac{dB}{dX}\right]$ x 100
99:1	159.69	a = 5.112	c = 13.234.	59	5.312	5.04	5.12

TEM Analysis

The morphologies of the as-prepared Fe_2O_3/Zn composite was characterized by Transmission Electron Microscopy and Selective Area Electron Diffraction pattern as shown in Figure 2a and 2b, the as-prepared Fe_2O_3 are uniform cube-shaped structures with the edge length of 200-400 nm. Figure 2a, demonstrates that most Fe_2O_3 nanoparticles tend to aggregate and a few of them are grown on the surface of Zn. Figure 2b indicates that the Fe_2O_3 nanoparticles are about 30 nm in diameter. It should be emphasized that, the presence of Zn and destroys the perfect cubic morphology of Fe_2O_3, but effectively decreases their particle size. Furthermore, Zn absolutely prevents Fe_2O_3 nanoparticles from agglomeration and enables a good dispersion of these oxide particles over the surface. It is believed that the doping and strong anchoring of Fe_2O_3 nanoparticles with Zn enable fast electron transport through the underlying layers to Fe_2O_3 nanoparticles to improve the electrochemical performance [20]. Fe^{3+} ions tend to occupy the spinel on A-site, which force Zn^{2+} ions on A-site to enter B-site. But the ionic radius of Zn^{2+} (0.083 nm) is larger than that of Fe^{3+} (0.067 nm), so the four oxygen atoms constituting tetrahedral site have to move outward along the diagonal of lattice to provide more space for Zn^{2+} ion.

The lattice parameter 'a' and 'c' was calculated using the relation, the results show that, the lattice parameter 'a' and 'c' shows the irregular trend with substitution of Zn. Since each primitive unit cell of the spinel contains 8 molecules, the value of X-ray density (dx) was determined according to the relation,

$$\mathbf{dx} = \frac{8M}{Na^3} \text{ ----------(1),}$$

where, N is the Avogadro's number (= 6.026 x 10^{23} atoms/mole) and M is the molecular weight of the sample.

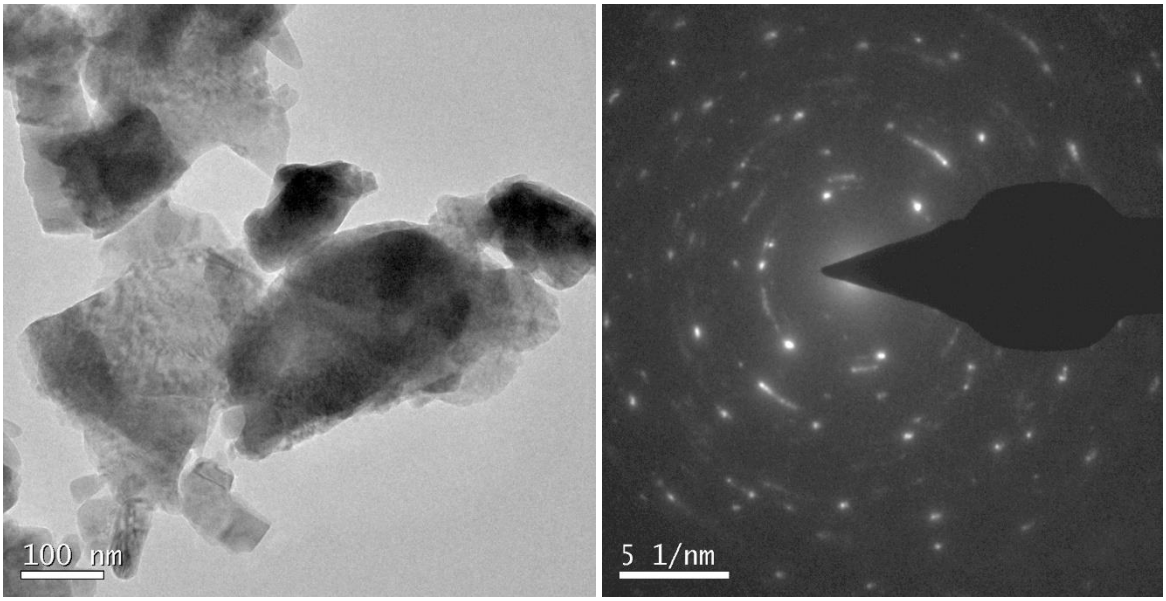

Figure 2(a-b) TEM and SAED Pattern of Fe_2O_3: Zn analysis

The bulk density was determined from mass and bulk volume of sample. The irregularity in both dx and dB with Zn content can be attributed to the atomic weight and the radii of constituent ions. The porosity (P) in % of the samples were calculated from dx and dB values using the expression,

$$P\% = 1 - \left[\frac{dB}{dX}\right] \times 100 \text{ ----------(2)}$$

$$D_{hk1} = \frac{0.94\lambda}{\beta Cos\theta} \text{ ----------(3)}$$

The crystallite size (D) of the particle of the powder was determined from XRD peak broadening of the (1 0 4) peak using Scherer formula equation (3), where, D_{hk1} is the mean dimension of the crystallite perpendicular to the plane (hkl), b is full width at half maximum in radians, h is the Braggs angle for the actual peak. The data on lattice constant (a), X-ray density (dx), bulk density (dB), porosity (P) and crystallite size is summarized in Table 3 [21].

SEM with EDAX analysis

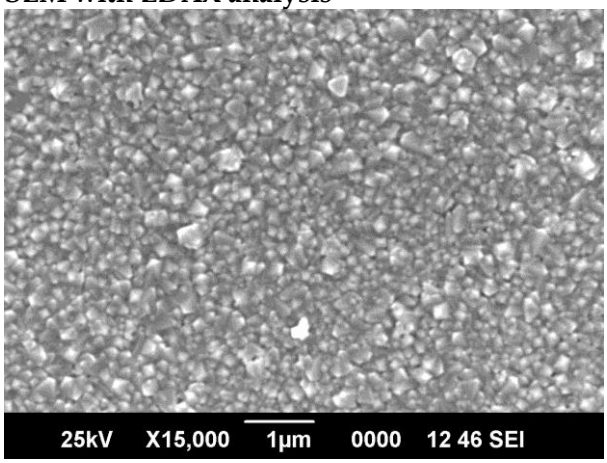

SEM has been used most for the characterization of nanocomposites structure, these microscopes have a resolution nearly 1 µm. The backscattered electrons are elastically scattered electrons and give compositional contrast depending on the atomic number of the specimen. These electrons have high energy and they come from the depth of the specimen (1 µm or more). SEM image of the topography of fractured surface nanoparticles shows; pattern of fractured surface just like the pattern appeared in fig. (3a) but the separation between the boundaries was lesser.

Element	Net Counts	ZAF	Weight %	Atom %	Formula
O	3921	3.750	26.60	50.64	O
Fe	18965	2.554	24.51	26.58	Fe
Zn	18532	1.122	48.89	22.78	Zn
Total			100.00	100.00	

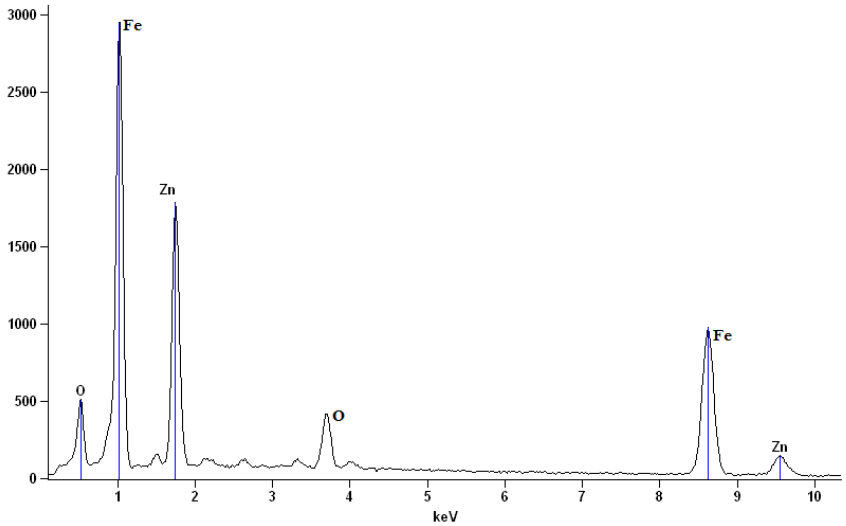

Figure 3(a-b): SEM with EDAX analysis of Fe_2O_3Zn

Magnetic Studies

Room temperature magnetization field dependence is shown in Figure 4 with the curve calculated according to the Langevin law taking into account the mean particle size from XRD. There is hysteresis in the experimental curve, the discrepancy between of the curves is observed that can be due to a wide distribution of particles size. At low temperatures, hysteresis loops occur, coercive field does not exceed 0.03 T at 3.8 K [22]. Spins pinned at the interface between ferromagnetic and anti-ferromagnetic components. Analogous vertical shifts of the hysteresis loops at low temperatures for core–shell Fe_2O_3Zn nanocomposites and ascribed it to the spin- like phase of an oxide shell at low temperatures. Vertical hysteresis loop shift was observed in the ensemble of Fe_2O_3Zn nanocomposite, and the shift value depended on the nanocomposite dimension [23].

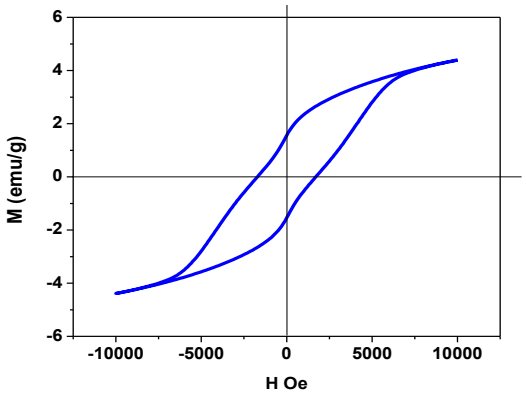

Figure 4: Ferroelectric behaviour of Fe_2O_3Zn nanocomposite

Conclusion

Magnetic nanoparticles formation in the glasses of the composite was shown to be responsible for their magnetic properties. Only one magnetic phase, Fe_2O_3Zn, has been detected independently of the large radius ions nature. At the same time, doping elements enhances the nanoparticle characteristics, including mean size, magnetization and magneto-optical effects. In particular, the nanocmposite size was found to depend on the doping element Zn concentration ratio, Zn, in such a way that there is an optimum concentration of these elements affording with larger magnetic particles.

References

1. Sivula, K., Le Formal, F. and Grätzel, M., 2011. Solar water splitting: progress using hematite (α-Fe_2O_3) photoelectrodes. Chem Sus Chem, 4(4), pp.432-449.

2. Chen, Jun, Lina Xu, Weiyang Li, and Xinglong Gou. α-Fe_2O_3 nanotubes in gas sensor and lithium-ion battery applications. Advanced Materials 17, no. 5 (2005): 582-586.

3. Kay, Andreas, Ilkay Cesar, and Michael Grätzel. "New benchmark for water photooxidation by nanostructured α-Fe_2O_3 films." Journal of the American Chemical Society 128, no. 49 (2006): 15714-15721.

4. Reddy, M. V., Ting Yu, Chorng-Haur Sow, Ze Xiang Shen, Chwee Teck Lim, G. V. Subba Rao, and B. V. R. Chowdari. "α-Fe2O3 nanoflakes as an anode material for Li-ion batteries." Advanced Functional Materials 17, no. 15 (2007): 2792-2799.

5. Rajeshwar, K., M. E. Osugi, W. Chanmanee, C. R. Chenthamarakshan, Maria Valnice Boldrin Zanoni, P. Kajitvichyanukul, and R. Krishnan-Ayer. "Heterogeneous photocatalytic treatment of organic

dyes in air and aqueous media." Journal of photochemistry and photobiology C: photochemistry reviews 9, no. 4 (2008): 171-192.

6. Woo, K., Lee, H.J., Ahn, J.P. and Park, Y.S., 2003. Sol–gel mediated synthesis of Fe2O3 nanorods. Advanced Materials, 15(20), pp.1761-1764.

7. El-Bahy, Z.M., Ismail, A.A. and Mohamed, R.M., 2009. Enhancement of titania by doping rare earth for photodegradation of organic dye (Direct Blue). Journal of Hazardous Materials, 166(1), pp.138-143.

8. Zhu, Q., Tao, F. and Pan, Q., 2010. Fast and selective removal of oils from water surface via highly hydrophobic core− shell Fe2O3@ C nanoparticles under magnetic field. ACS applied materials & interfaces, 2(11), pp.3141-3146.

9. Malato, S., Fernández-Ibáñez, P., Maldonado, M.I., Blanco, J. and Gernjak, W., 2009. Decontamination and disinfection of water by solar photocatalysis: recent overview and trends. Catalysis Today, 147(1), pp.1-59.

10. Rao, A.N., Sivasankar, B. and Sadasivam, V., 2009. Kinetic studies on the photocatalytic degradation of Direct Yellow 12 in the presence of ZnO catalyst. Journal of Molecular Catalysis A: Chemical, 306(1-2), pp.77-81.

11. Seddigi, Z.S., 2010. Removal of alizarin yellow dye from water using zinc doped WO 3 catalyst. Bulletin of environmental contamination and toxicology, 84(5), pp.564-567.

12. Rauf, M. A., and S. Salman Ashraf. "Radiation induced degradation of dyes—an overview." Journal of hazardous materials 166, no. 1 (2009): 6-16.

13. Yang, Hongwei, and Hefa Cheng. Controlling nitrite level in drinking water by chlorination and chloramination. Separation and Purification Technology 56, no. 3 (2007): 392-396.

14. Lu, Jinfeng, Tao Zhang, Jun Ma, and Zhonglin Chen. "Evaluation of disinfection by-products formation during chlorination and chloramination of dissolved natural organic matter fractions isolated from a filtered river water." Journal of Hazardous Materials 162, no. 1 (2009): 140-145.

15. Coleman, H. M., C. P. Marquis, J. A. Scott, S-S. Chin, and R. Amal. Bactericidal effects of titanium dioxide-based photocatalysts. Chemical Engineering Journal 113, no. 1 (2005): 55-63.

16.

17. Kaviyarasu, K., N. Geetha, K. Kanimozhi, C. Maria Magdalane, S. Sivaranjani, A. Ayeshamariam, J. Kennedy, and M. Maaza. "In vitro cytotoxicity effect and antibacterial performance of human lung epithelial cells A549 activity of zinc oxide doped TiO_2 nanocrystals: investigation of bio-medical application by chemical method. Materials Science and Engineering: C 74 (2017): 325-333.

18. Gaya, Umar Ibrahim, and Abdul Halim Abdullah. "Heterogeneous photocatalytic degradation of organic contaminants over titanium dioxide: a review of fundamentals, progress and problems." Journal of Photochemistry and Photobiology C: Photochemistry Reviews 9, no. 1 (2008): 1-12.

19. Gupta, A.K. and Gupta, M., 2005. Synthesis and surface engineering of iron oxide nanoparticles for biomedical applications. biomaterials, 26(18), pp.3995-4021.

20. Mehra, O.P. and Jackson, M.L., 2013. Iron oxide removal from soils and clays by a dithionite–citrate system buffered with sodium bicarbonate. In Clays and clay minerals (pp. 317-327). Pergamon.

21. Ezhilarasi, A. Angel, J. Judith Vijaya, K. Kaviyarasu, M. Maaza, A. Ayeshamariam, and L. John Kennedy. "Green synthesis of NiO nanoparticles using Moringa oleifera extract and their biomedical applications: Cytotoxicity effect of nanoparticles against HT-29 cancer cells." Journal of Photochemistry and Photobiology B: Biology 164 (2016): 352-360.

22. Zhong, L.S., Hu, J.S., Liang, H.P., Cao, A.M., Song, W.G. and Wan, L.J., 2006. Self-Assembled 3D flowerlike iron oxide nanostructures and their application in water treatment. Advanced Materials, 18(18), pp.2426-2431.

23. Gupta, V.K., Agarwal, S. and Saleh, T.A., 2011. Chromium removal by combining the magnetic properties of iron oxide with adsorption properties of carbon nanotubes. Water research, 45(6), pp.2207-2212.

24. Helan, V., J. Joseph Prince, Naif Abdullah Al-Dhabi, Mariadhas Valan Arasu, A. Ayeshamariam, G. Madhumitha, Selvaraj Mohana Roopan, and M. Jayachandran. "Neem leaves mediated preparation of NiO nanoparticles and its magnetization, coercivity and antibacterial analysis." Results in physics 6 (2016): 712-718.

Cite this article as:

Kavin Micheal M., Ayeshamariam A., Alhaji N.M.I., Fowziya S.A., Rajasekar S. and M. Jayachandran. Ferroelctric behaviour of Fe2O3Zn Nnaocomposites. *International Journal of Bio-Pharma Research*, Volume 8, Issue 5 (2019) pp. 2575-2581.

http://dx.doi.org/10.21746/ijbpr.2019.8.5.4

Source of support: Nil**; Conflict of interest:** Nil